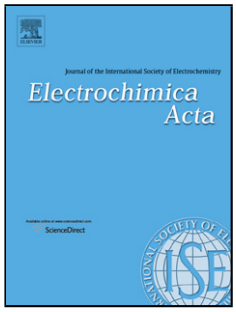

Title: An experimental study of pH distributions within an electricity-producing biofilm by using pH microelectrode

Authors: Junxian Hou, Zhongliang Liu, Yu Zhou, Wenwen Chen, Yanxia Li, Lixia Sang

PII: S0013-4686(17)31744-9
DOI: http://dx.doi.org/10.1016/j.electacta.2017.08.101
Reference: EA 30105

To appear in: *Electrochimica Acta*

Received date: 18-2-2017
Revised date: 22-7-2017
Accepted date: 16-8-2017

Please cite this article as: Junxian Hou, Zhongliang Liu, Yu Zhou, Wenwen Chen, Yanxia Li, Lixia Sang, An experimental study of pH distributions within an electricity-producing biofilm by using pH microelectrode, Electrochimica Actahttp://dx.doi.org/10.1016/j.electacta.2017.08.101

An experimental study of pH distributions within an electricity-producing biofilm by using pH microelectrode

Junxian Hou, Zhongliang Liu*, Yu Zhou, Wenwen Chen, Yanxia Li, Lixia Sang

Key Laboratory of Enhanced Heat Transfer and Energy Conservation, Ministry of Education, College of Environmental and Energy Engineering, Beijing University of Technology, Beijing 100124, China

*Corresponding author: liuzhl@bjut.edu.cn (Z.L. Liu)

Graphical abstract

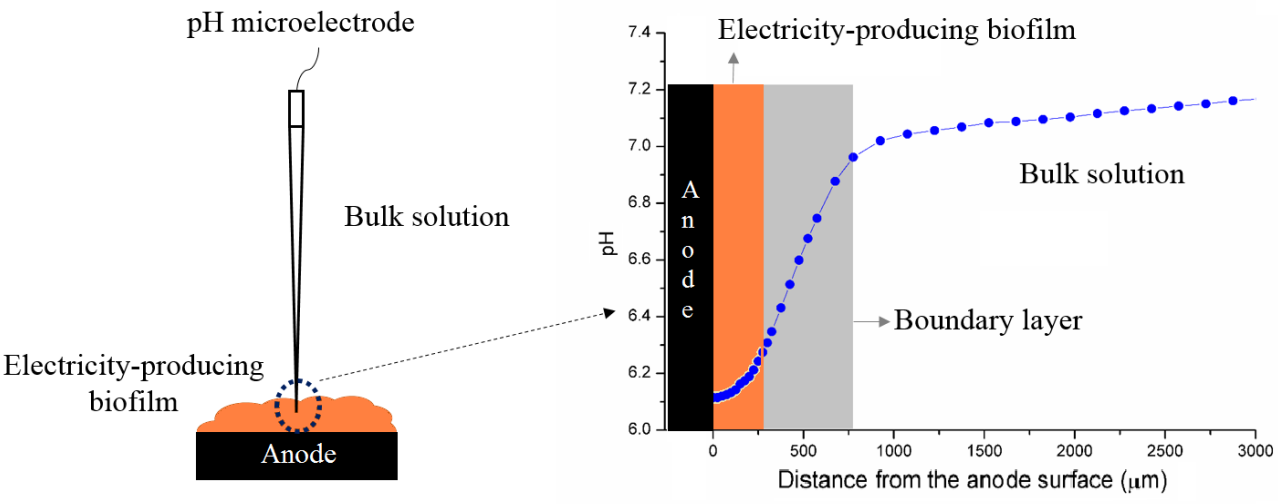

Highlights

- This study quantified the spatial pH distributions within the *Geobacter* biofilm.
- The detected pH level was as low as 5.57 in a 350μm thick *Geobacter* biofilm.
- The average pH levels within *Geobacter* biofilm decreased over time.

Abstract: This study quantified the spatial pH distributions within an electricity-producing biofilm and its concentration boundary layer, as well as the bulk solution by employing pH microelectrode. The relationship between pH distributions and current densities was explored. It was found that (1) pH level near the anode surface was detected as low as 5.57 compared to 6.90 of the bulk solution across a 350μm thick *Geobacter* biofilm; (2) the average pH levels within the biofilm decreased over time; (3) pH variations within the biofilm shifted the

midpoint potential of Cyclic Voltammetry with 59.0 mV per pH; (4) pH level near the anode surface was as low as 4.91 for a 25 mM phosphate buffer solution compared to 5.73 of that for the 100 mM. Furthermore, a method was recommended to estimate the thickness of biofilm by plotting the derivative of pH-depth profile.

Keywords: pH distribution; pH microelectrode; *Geobacter*; biofilm thickness; concentration boundary layer

1. Introduction

Electricity-producing biofilms respire in a unique way that utilizing solid external materials as terminal electron acceptors for their metabolism which is of interest as catalysts in bioelectrochemical systems (BESs), such as microbial fuel cells (MFCs) and microbial electrolysis cells (MECs), as well as desalination, bioremediation and sensing systems [1-4]. Anode-respiring bacteria (ARB) use the anodes of MFCs, MECs or other bioelectrochemical systems for respiration and ultimately transfer electrons from microorganisms to the anodes. The electrical current of anodic biofilm occurs as a result of redox reaction that anodes occurs oxidation reaction where the substrate like acetate or other organic substances is consumed. In this process, protons are released to the anolyte, and electrons are transferred to the anode [5, 6], as shown in Eq. 1.

$$CH_3COO^- + 4H_2O \rightarrow 2HCO_3^- + 9H^+ + 8e^- \quad (1)$$

Electron transfer must be companied with proton transfer to maintain solution electrically neutral, which is expected to cause pH gradients outside and inside the electricity-producing biofilm. Moreover, higher current generation may lead to larger proton accumulation which instead could be inhibitory to the growth as well as the electron generation of the anodic biofilms [7-9]. As we all know that pH plays a critical role in determining the performance of electricity-producing biofilms, therefore, the pH distributions inside the biofilm is of great importance for understanding the mechanism of electron producing and transport in

BESs.

Most of the studies concerning the influences of pH change on the anodic biofilms were limited to the bulk solution. It was demonstrated that current density increased with higher buffer concentration, indicating that the current density was limited by the proton transport out of the biofilm [5]. Franks *et al*. demonstrated that as the bulk pH was changed from 6.9 to 6.15, the current was decreased by 50% when employing *Geobacter sulfurreducens* as the anodic biofilm [10]. To better understand proton transfer mechanisms, mathematical models have been also established to predict proton transport in electrochemical active biofilms (EABs). It was predicted a pH variation of 0.03 units in a 100 μm thick anodic biofilm [11]. Marcus *et al*. predicted a pH change of 1.5 units across over a 450 μm anodic biofilm for 15 A m^{-2} [7-8]. The pH values at 4 different depths inside the *Geobacte*r biofilm were measured by introducing a pH-sensitive fluoroprobe. It was found that the pH level near the anode surface was 6.1 compared to 7 in the external medium [10]. Babauta *et al.* measured a pH drop from 6.8 to 6.5 at a current of 1.05 mA and from 6.9 to 6.3 at 1.85 mA within the *Geobacter* biofilm by microelectrode [12]. These studies proved the importance of pH distributions inside electricity-producing biofilms. Therefore, it is still not clear how current density and pH distribution inside the anodic biofilms are related to each other. Protons generation by cells and their transport out of the anodic biofilms, are supposed to result in the formation of a proton gradient across the biofilm. The formation of pH gradients across the biofilm depth would cause the reduced performance of the inner microorganisms and also affect their growth [13]. So understanding the detailed characteristics of the pH distributions inside the microscale biofilm and their influences on the electricity-producing performance are critical for improving better-performance anodes.

The goal of this study is to quantify the spatial and temporal pH distributions and variation across the electricity-producing biofilm depth. The relationship between pH distributions and current densities was also explored. *Geobacter* spp is an excellent candidate for electricity-producing bacteria as it can convert acetate to electrons on anodes and the electron transfer believed is direct [3, 11, 12, 14]. The pH-depth profiles inside the *Geobacter* biofilm were obtained by pH microelectrode which allowed for noninvasive, nondestructive, high spatial resolution and real-time measurements in living biofilms. Finding the above conditions is dependent upon understanding the microscale conditions inside anodic biofilms, which have not been reported so far as the present authors could know. Moreover, a method was recommended to estimate the thickness of the biofilm and the boundary layer by plotting the derivative of pH-depth profile.

2. Materials and Methods

2.1 Bioreactor

As shown in Fig. S1 of the Supplementary Material, electricity-producing biofilm was grown on the working electrode in a three-electrode bioreactor (300 mL) under the constant applied potential (-0.1 V vs Ag/AgCl). Carbon cloth (0.36±0.02mm thick) with a projected surface area of 2.4cm^2 (2.0 cm×1.2 cm) and oversized Pt mesh (2.0 cm×2.0 cm) were served as the working and counter electrodes, and the reference electrodes were Ag/AgCl (3 M KCl, Leici Instruments, Shanghai, China). Carbon cloth was purchased from Shanghai Hesen Electric Co., Ltd and Pt meshes from Tianjin Aida Hengsheng Technology Co. Ltd. The inoculum for this bioreactor was obtained from an acetate-fed MFC that had operated continuously for more than 6 months and had a *Geobacter*-enriched bacterial community (65%) originally from Beijing Gaobeidian Wastewater Treatment Plant. During initial inoculation, the growth medium flow was stopped for 24 h to encourage the attachment of bacteria to the working electrode.

Thereafter, the anaerobic, nitrogen-purged, acetate-containing medium was circulated through the reactor with a hydraulic retention time of 5 h. Acetate was used as the electron donor and the working electrode was as the electron acceptor. All experiments were carried out in a 35±0.5 °C incubator. The growth medium consisted of CH_3COONa (1.64 g L^{-1}), NaCl (0.1 g L^{-1}), NH_4Cl (0.5 g L^{-1}), $MgSO_4 \cdot 7H_2O$ (0.1 g L^{-1}), $CaCl_2 \cdot 2H_2O$ (0.02 g L^{-1}), 10 mL L^{-1} Wolfe's vitamin solution [12] and 50 mM phosphate buffer. After every pH and CV measurement, the medium in the bioreactor was poured out in order to remove the suspended bacteria accumulation on the inside wall of the bioreactor. Then the fresh growth medium was circulated again. Furthermore, a group of replicated experiments were also carried out.

2.2 Calibration of pH microelectrode

pH microelectrodes (Unisense, Denmark) were used to characterize the pH distributions within the anodic biofilm. The diameter of the microelectrode tip is 50 μm. Prior to each measurement, the pH microelectrode was calibrated using commercial buffer solutions (pH=4.01, 6.86 and 9.18). Linear calibration curves were obtained with a slope in the range of -58.10 ~ -58.80 mV/pH. The calibration data were presented in Table S1 and Fig. S2. Post-calibration was also performed in the same way after every measurement.

2.3 pH microelectrode measurement

pH measurements were performed under operating conditions. The ports were opened by removing the rubber stopper above the biofilm anode for inserting microelectrode and its reference electrode. Pure N_2 was continuously purged into the headspace to minimize oxygen intrusion into the system from the open port. Initially, the pH microelectrode tip was put into bulk solution several thousands of micrometers above the biofilm surface, and then gradually moved downwards step by step (50-200 μm increments outside the biofilm and 25μm increments inside the biofilm) regularly controlled by SensorTrace Profiling software

on the computer and the pH values were recorded simultaneously, when passing through the bulk solution, the concentration boundary layer and finally reaching the bottom of the biofilm (the surface of the anode).

3. Results and Discussion

3.1 *Geobacter* biofilm growth

Fig. 1 shows the current generation of *Geobacter* biofilm on the carbon cloth-based anode under constant potential (-0.1 V, *vs.* Ag/AgCl) as a function of time. The red arrows indicate the current at which the pH and CV were measured during the biofilm growth. From this figure, one can see that the current density reached to 1.07 A m^{-2} after 45 h inoculation as indicated by the first red arrow. As the bacteria or biofilm attachment increased, the current density showed an upward trend up to 5.89 A m^{-2} after 256 h inoculation. Thereafter, the electricity-producing capability of the *Geobacter* biofilm was further improved as time elapsed. It is worth to point out that the maximum current density increases surprisingly to 10.71 A m^{-2} after 440 h growth. After that it took a steady downward trend. Then the medium was replaced by fresh anolyte and circulated again at 462 h. It can be seen that the current commenced again and reached the maximum of 10.70 A m^{-2}, and was almost equal to the previous maximum current density which simply implied that the deep biofilm growth would be restricted by the shortage of substrate or proton accumulation (low pH) as they were inhibitory to the biofilm activity when operating at large current for a long time. After 576 h operation, the anode-respiring biofilm was extracted for biodiversity analysis. The result of 16S rRNA analysis showed that *Geobacter spp* accounted for 74%, as shown in Fig. S3(a). The replicated experiments were also finished and the results clearly showed that the bio-anode got a similar current density with the one here, as shown in Fig. S1(c). And the biodiversity analysis indicated that *Geobacter spp* accounted for 65% in Fig. S3(b).

3.2 *In situ* pH distributions within *Geobacter* biofilm

To quantify the real-time pH distributions across the *Geobacter* biofilm depth, the pH-depth profiles were obtained using the pH microelectrode. They were measured at different current levels, as the red arrows indicated in Fig 1. The pH microelectrode tip was initially put into bulk solution several thousands of micrometers above the biofilm surface, and then gradually moved downwards step by step. At least 3 locations upon the biofilm were selected for pH measurements for each current density considering the irregularity of the biofilm surface, the measured data is shown in Fig. S4. The averaged pH-depth profiles for each current density were calculated and depicted in Fig. 2(a)~(e). It was found that there was a small region that was closed to the very vicinity of 0 μm in each pH-depth profile (Fig.2) where the measured pH value changed only a little or almost kept a constant. This would indicate that the microelectrode tip had already entered into the vicinity of the electrode surface. Therefore, this small region was assumed to be located near the bottom of the biofilm. In Fig. 2, the bottom of the biofilm (the electrode surface) is at the depth of 0 μm. As it was expected, the pH decreased gradually as the microelectrode tip was moved from the bulk solution (～3500 μm) towards the anode surface (0 μm) regardless of biofilm age for all profiles. Fig. 2(f) presents one of the pH-depth profiles measured at 7.93A m^{-2} and its corresponding proton concentration depth (PC-depth) profile. One can clearly see from this figure that the pH curve is sigmoid-shaped and the PC curve zigzag-shaped. Actually, "S" and "Z" shapes always existed in all our experiments. Close observation of Fig. 2(a)~(e) showed that the pH distributions along the depth could be divided into three typical regions, *i.e.*, the anodic biofilm, the concentration boundary layer and the bulk solution. These three regions display different characteristics due to their different main functions. As we know, pH is expected to be around a constant in the bulk solution due to the fact that in this region there is no microbial nutrient removal and buffer

solution influence which is of a similar trend as the substrate and/or oxygen distribution in bio-systems [14, 15]. In Fig. 2, a steep slope always appeared between 750 and 1300μm in all profiles, which was actually the interface located between the boundary layer and the bulk solution and this sharp decrease also indicated that the pH microelectrode tip was passing through the interface layer from the bulk and then the boundary layer and the electricity-producing biofilm afterwards.

3.3 Thickness of *Geobacter* biofilm

In bioelectrochemical systems, it was demonstrated that the protons were transported out of the anodic biofilm mainly by protonating the conjugate base of the buffer system (*i.e.*, $HPO_4^{2-} + H^+ \rightarrow H_2PO_4^-$) [5]. The pH data obtained using the pH microelectrode actually reflected the concentration of the uncomplexed proton (free proton) only [5]. Marcus *et al*. developed a platform for anodic biofilm modeling describing simultaneous phenomena of electrical neutrality, ARB half reaction, diffusion, migration and acid-base chemistry [7, 8]. Their results showed that the pH development had an approximately linear relationship with depth within the boundary layer, and an exponential relation within the biofilm, which was consistent very well with our experimental result in Fig. 2. As we know, the pH value should have the biggest decrease when the pH microelectrode starts to pass through the biofilm from the concentration boundary layer. So a maximum gradient (a turning point) would appear at the interface of the biofilm and the concentration boundary layer. The mechanism behind this was simple. The protons were produced inside the biofilm by consuming the substrate that was diffused from the concentration boundary layer, this of course would create the largest the proton or pH gradient at that interface. Therefore, by calculating the first derivative of each pH to the depth in pH-depth profiles, one may identify the location of the boundary of the biofilm or the interface according to the slope trend. In this way, the thickness of anodic

biofilm and the boundary layer could be estimated.

Taking the pH-depth profiles at 7.93 Am^{-2} as an example, 5 locations were chosen for pH measurement there. Their first-order derivative plots were presented in Fig. 3(a). After averaging these plots, the averaged derivative plots were obtained as the inset shown. It can be clearly seen that the slope in the bulk solution, boundary layer and *Geobacter* biofilm was completely different. The derivatives kept around zero in the bulk solution because pH value here was approximately a constant, and then the derivatives departed from zero which reflected the fact that the microelectrode was moved downwards step by step into the boundary layer. After that, it gradually increased to the slope of ~1.5×10^{-3} pH/μm until it acquired its maximum slope. It can be found that the derivatives in the boundary layer did not keep constant which was possibly caused by the planktonic bacteria there. Actually, the location with the maximum slope was the interface between anodic biofilm and the boundary layer. This is because the electricity current or the proton H^+ was actually produced within the biofilm and the substrate got contacted at this interface. It can be expected, due to the diffusion effect of H^+ and the substrate, the gradient of H^+ and therefore that of pH value tends to decrease at the locations away from the interface of the anodic film and the boundary layer. Inside the *Geobacter* biofilm, the slope decreased sharply until reaching the bottom of the biofilm due to the decreased effective diffusion coefficient inside it. As one can see clearly, the turning point with the maximum slope in the inset was at the depth of about 275 μm which was therefore the biofilm thickness $\delta_{biofilm}$. Metabolically inactive biofilm layer could also be detected from the fact that the pH value in this region presented an opposite trend compared with the active biofilm. As shown in Fig. 2(*d*) and Fig. 2(*e*), in the vicinity of the anode surface, the pH value either remained a constant of a low value or decreased with the depth. This implied that the protons here were mainly transported from the outer active cells. And this also explained why

the derivatives of this region were equal to or less than zero.

It should be stressed that we actually developed a method here to estimate the biofilm thickness using the measured pH-depth profiles that extends the whole range from the anode surface to the bulk solution. To describe it more clearly, the method is summarized as follows: (1) With the help of the pH microelectrode, the pH distributions along the depth direction of the biofilm at different positions perpendicular to the depth direction at a given biofilm growth stage are obtained; (2) Using the pH distributions obtained at a given biofilm growth stage, the first derivatives of pH to depth are calculated; (3) Calculate the average first derivative from the first derivatives obtained in (2); (4) The average first derivative is plotted against the depth; (5) The depth at which the average first derivative acquires its maximum is defined as the biofilm thickness or the interface of the biofilm and the boundary layer. (6) The right hand side of the interface belongs to that between the boundary layer and the bulk solution. This thickness is something arbitrary. Here we define this thickness as the distance needed for the average first derivative reduces from its maximum to 1% of its maximum. (7) The biofilm can be further divided into the active and the inactive part. The inactive part of the biofilm is the region near the anode where the average first derivative of pH is very small or of a negative value. The thickness of the inactive part could be determined by reading the corresponding pH-depth distributions. The thickness of the active part is equal to the thickness of the biofilm minus the thickness of the inactive part.

Using the method described above, the first derivative plots at other current densities were obtained in Fig. S5(*a*)~(*h*). The insets are the average first-order curves for each current density. Fig. 3(b) summarizes the *Geobacter* biofilm thickness included the inactive part and the active part. As can be seen from this figure, the biofilm thickness kept going up. It was about 90 μm at 1.27 A m^{-2} and became 190 μm if the current increased to 2.97 A m^{-2}. It increased greatly over time in the first 285 h inoculation which meant that the attached

bacteria/biofilm increased over time. It reached a thickness of 275 μm at 7.93 A m^{-2}. After that, the development of the active biofilm slowed down and then it reached 300 μm at 9.25 A m^{-2} with a partial inactive biofilm layer around 25 μm. We found that the thickness of the active biofilm layer kept at about 275 μm almost unchanged later on, indicating that its thickness had already reached its maximum value due to the availability of the substrate or low pH near anode biofilm. Therefore, we would say that the top 275 μm from the surface of the anodic biofilm that produced protons and consumed acetate was metabolically active. The detected inactive biofilm thickness increased to about 50μm at 10.71 A m^{-2} and 75 μm at 10.23 A m^{-2}. This result proved that the cells near the electrode formed a dense inactive layer and would be acetate-limiting or/and pH-inhibiting, as it was demonstrated that the effective diffusion coefficient in the vicinity of the electrode decreases greatly compared with the outer biofilm inside a 370 μm *Geobacter* biofilm [17]. However, extracellular electron transport of the biofilm was not prevented by the inactive regions, even when the biofilm was hundreds of microns thick because the conductivity was large enough for cells to transfer electrons across this region [18]. This explained why the current density did not decrease even the inactive region existed. In this study, the boundary layer thickness varied in the range of 450-650 μm.

3.4 pH variations near anode surface and in the bulk solution

From Fig. 2, one can see that pH values near the anode surface and in the bulk solution gradually decrease as the biofilm ages. It was clear that the real-time pH values at a given location decreased as the current increased, which meant that more and more protons had accumulated inside the biofilm over time. To see this tendency more clearly, Fig. 4(a) presents them as a function of current density. At the bottom of biofilm, pH was around 7.33 at a current density of 1.07 A m^{-2}, and became 6.57 at 4.46 A m^{-2}, it continued to drop down to 6.12 at 7.93 A m^{-2}, and reached to an even-lower value of 5.72 with the maximum current

density of 10.71 A m^{-2} after 440 h growth. However, after that, the biofilm bottom pH decreased to its lowest value of 5.57 at the declining current (10.23 A m^{-2}) at 455h. It went up a little to 5.63 as the medium was changed at 482h (10.70 A m^{-2}). Furthermore, in the bulk solution, pH levels showed a decreasing trend as well. It decreased from 7.40 at 1.07 A m^{-2} and to 6.90 at 10.23 A m^{-2} due to the fact that the free protons were transported from the inner biofilm to the bulk through the boundary layer. Overall, in a 350μm thick *Geobacter* biofilm (10.23 A m^{-2}), the detected pH level near the anode surface was as low as 5.57 compared to 6.90 of bulk solution.

Let us return to Fig. 4(a) again. The pH difference between the bulk solution and the anode surface was calculated. The difference increased with the current density due to the fact that the larger current density and thus the thicker biofilm would certainly lead to the heavier proton accumulation. One can find that the pH difference was only 0.11 pH units at 1.27 A m^{-2}. It increased to 0.63 at 5.89 A m^{-2}. If the current density was 10.71 A m^{-2}, then the pH difference was further increased to 1.06 of which the corresponding bulk layer and biofilm bottom pH value was 6.78 and 5.72 respectively. This means that the proton concentration near the electrode surface was almost 11.5-fold higher than that of the bulk layer. It also can be found that the pH difference increased almost linearly with the current density (r^2=0.98), as shown in Fig. S6. After operating at a large current over a long time, the pH difference reached its maximum value of 1.33 units at 10.23 A m^{-2} which means that the proton concentration near the electrode surface was almost 20-fold higher than that of the bulk solution.

3.5 Average pH within *Geobacter* biofilm

Based on the biofilm thickness and proton concentration depth profiles, the average proton concentration within the *Geobacter* biofilm can be calculated by the following equation,

$$\overline{C_{H^+}} = \frac{1}{\delta_{biofilm}} \int_0^{\delta_{biofilm}} C_{H^+} dx \quad (3)$$

For example, by integrating the shadow area in the inset shown in Fig. 2(f), it can be easily calculated that the average proton concentration within the biofilm. Then the average pH can be obtained from it. In this way, the average pH within the anodic biofilm could be determined for different current density conditions. Based on the data in Fig 2, the calculated average pH values are 7.29, 7.01, 6.91, 6.48, 6.20, 6.00, 5.88, and 5.61 for 1.27 A m^{-2}, 2.58 A m^{-2}, 2.97 A m^{-2}, 5.89 A m^{-2}, 7.93 A m^{-2}, 9.25 A m^{-2}, 9.83 A m^{-2} and 10.23 A m^{-2}, respectively. Fig. 4(b) presents the variation curve for the average pH within the biofilm as well as the corresponding proton concentration curve. One can see that the average pH value decreased with the current density, which was simply a result of the proton accumulation inside the biofilm. Then it followed a big decrease after operating at large current for a long time. Before that, it discloses that the average pH value across the biofilm was a linear function of the current density at a level as high as r^2=0.99, as the inset shown in Fig. 4(b). This finding may be used to estimate the average pH of the *Geobacter* biofilm according to the current density. It can also be observed that the average proton concentration increases steadily with the current density, then following a big increase. It can be also found that the average pH inside the biofilm decreased with the biofilm thickness. It dropped from 7.29 to 5.88 as the biofilm thickness increased from 90 μm to 325 μm, and followed a sharp decrease to 5.61 in the 350 μm thick biofilm. This means that the detected free protons accumulated inside the *Geobacter* biofilm increased to 26-fold (1.41 pH units) compared with the primary biofilm when the biofilm thickness increased from 90 μm to 325 μm, and even 48-fold (1.68 pH units) when the biofilm thickness reached to 350 μm, certifying that protons could not be transported out of the biofilm effectively with a thickness of 350 μm under a 50 mM phosphate buffer condition.

3.6 Cyclic Voltammetry

CVs were recorded after pH measurements, as shown in Fig. S7. All CVs displayed a typical sigmoidal shape after the bioreactor initiation which was similar to the responses reported for acetate oxidation in *Geobacter*-dominated biofilms [19, 20]. The first-order derivatives of CVs were used to check the midpoint potential, as shown in Fig. 5. As one can see from this figure, there was one major redox couple of the acetate oxidation and the midpoint potential of CVs was shifted slightly from the left to the right as the current density increased. The redox couple was centered at -0.425 V vs. Ag/AgCl at 1.27 A m^{-2} with an average pH value of 7.29 inside the *Geobacter* biofilm, and as the current increased to 5.89 A m^{-2}, it centered at -0.357 V with an average pH value of 6.48. And the midpoint potential finally increased to -0.328 V vs. Ag/AgCl with an average pH of 5.71 at 10.70A m^{-2}. From these results one could well conclude that the midpoint potential increases gradually as the pH inside the biofilm decreases. The inset in Fig. 5 depicted the midpoint potential curve as a function of the average pH within the biofilm. A least square regression was carried out and it showed that they were in a good linear relation. The slope of the fit line was 59.0 mV per pH shift, which was closed to its theoretical value (59.2 mV per pH) of Nernst equation. The main reason for this change would be that the electron transfer process here is proton coupled or dependent, which means that the complex mechanism of electron transfer from a bacterium, coupled to redox and proton-pumping cascade in the bacterial metabolism, is pH dependent [20,21]. Therefore, it can be well concluded that a slight change in the average pH within the *Geobacter* biofilm will result in a large fluctuation in the midpoint potential. In return, the change of the midpoint potential also examines that the pH values inside the biofilm continuously vary with current density.

3.7 Effect of buffer concentration on pH distributions

Buffer solutions were always used to reduce proton accumulation within the biofilm clusters in BESs [22-25]. In order to further evaluate the effects of buffer concentration on the pH distributions and current generation within the *Geobacter* biofilm, the experiments under various buffer concentration medium (50 mM, 75 mM, 100 mM, 50 mM and 25 mM) were carried out in turn. The 50mM solution was fed into the reactor twice to ensure the activity of the *Gerobacter* biofilm. All inflow was of a constant pH of about 7.35~7.50 throughout the experiments. Fig. S8 presents the current curves under various buffer concentration conditions. The current density was 10.73 A m^{-2}, 12.5 A m^{-2}, 16.50 A m^{-2}, 9.80 A m^{-2}, and 6.01 A m^{-2} for 50 mM, 75 mM, 100 mM, 50 mM and 25 mM phosphate buffer inflow, respectively. As one can see that the current density increased with the buffer concentration.

For pH measurement, at least 3 locations upon the biofilm were selected for each buffer condition, the measured data is displayed in Fig. S9. Fig. 6 presents the calculated average pH distributions. The pH value near the anode surface was about 4.91 for 25 mM, which was significantly smaller than that of 50 mM, 75 mM and 100 mM whose pH near the anode surface was 5.31, 5.82 and 5.73, respectively. This demonstrated that under low buffer concentration conditions, the protons would not be effectively transported out of the biofilm and the cells activity as well as current generation was severely limited. After 576 h incubation, the *Geobacter*-biofilm-covered anode was taken out from the bioreactor. Fig. S10 is the digital photograph after removing half of the biofilm from the electrode surface for comparison.

4. **Conclusions**

This study investigated the spatial pH distributions inside the *Geobacter* biofilm at different current densities by employing pH microelectrode. In a 350μm thick *Geobacter* biofilm (10.23 A m^{-2}), the detected pH level in the vicinity of anode surface was as low as 5.57 compared to 6.90 of the bulk solution. Herein, the pH difference reached its maximum value of 1.33 units which means that the proton concentration near the electrode surface was almost 20-fold higher

than that of the bulk solution. This study also demonstrates that the protons could not be effectively transported out of the biofilm under low buffer concentration conditions in a thick biofilm.

Acknowledgments

This work is supported by the Chinese National Natural Science Foundation Project (No. 51676004).

References

[1] E. H. Yu, S. A. Cheng, K. Scott, B. Logan, Microbial fuel cell performance with non-Pt cathode catalysts, Journal of Power Sources, 171 (2007), 275-281

[2] C. Santoroa, F. Soavib, C. Arbizzanib, A. Serova, S. Kabira, K. Carpenterc, O. Bretschgerc, P. Atanassova. Co-generation of hydrogen and power/current pulses from supercapacitive MFCs using novel HER iron-based catalysts, 220 (2016), pp. 672–682

[3] J. T. Babauta, R. Renslow, Z. Lewandowski, H, Beyenal, Electrochemically active biofilms: facts and fiction. A review, Biofouling, 28(2012), pp. 789-812

[4] J. Chouler, I. Bentley, F. Vaz, A. OrFee, M. D. Lorenzo, Exploring the use of cost-effective membrane materials for Microbial Fuel Cell based sensors, Electrochimica Acta, *http://dx.doi.org/10.1016/j.electacta.2017.01.195*

[5] I. Torres, A. K. Marcus, B. E. Rittmann, Proton transport inside the biofilm limits electrical current generation by anode-respiring bacteria, Biotechnol. Bioeng., 100(2008), pp. 872-881

[6] B. E. Logan, B. Hamelers, R. Rozendal, U. Schröder, J. Keller, S. Freguia, P. Aelterman, W. Verstraete, K. Rabaey, Microbial Fuel Cells: Methodology and Technology, Environ. Sci. Technol., 40(2006), pp. 5181–5192

[7] A. K. Marcus, C. I Torres, B. E. Rittmann, Evaluating the impacts of migration in the biofilm anode using the model PCBIOFILM, Electrochim. Acta,55(2010), pp. 6964-6972.

[8] A. K. Marcus, C. I Torres, B. E. Rittmann, Analysis of a microbial electrochemical cell using the proton condition in biofilm (PCBIOFILM) model, Bioresour. Technol., 102(2011), pp. 253-262

[9] M. H. Qin, Ibrahim M. Abu-Reesh, Z. He, Effects of current generation and electrolyte pH on reverse salt flux across thin film composite membrane in osmotic microbial fuel, Water Res., 105(2016), pp. 583-590

[10] A. E. Franks, K. P. Nevin, H. F Jia, M. Izallalen, T. L. Woodard, D. R. Lovley, Novel strategy for three-dimensional real-time imaging of microbial fuel cell communities: monitoring the inhibitory effects of proton accumulation within the anode biofilm, Energy Environ. Sci., 2(2009), pp. 113-119

[11] C. Picioreanu, M. C. van Loosdrecht, T. P. Curtis, K. Scott, Model based evaluation of the effect of pH and electrode geometry on microbial fuel cell performance, Bioelectrochemistry, 78(2010), pp. 8-24

[12] J. T. Babauta, H. D. Nguyen, T. D. Harrington, R. Renslow, H. Beyenal, pH, redox potential and local biofilm potential microenvironments within Geobacter sulfurreducens biofilms and their roles in electron transfer, Biotechnol. Bioeng, 109(2012), pp. 2651-2662

[13] Z. Lewandowski and H. Beyenal, 2013 Fundamentals of Biofilm Research, 2nd ed. CRC Press

[14] E. Atci, J. T. Babauta, S. T. Sultana, H. Beyenal, Microbiosensor for the detection of acetate in electrode-respiring biofilms, Biosens. Bioelectron., 81(2016), pp. 517-523

[15] X. H. Zhou, Y. Tong, H. H. Shi, H. M. Shi, Temporal and spatial inhibitory effects of zinc and copper on wastewater biofilms from oxygen concentration profiles determined by microelectrodes, Water Res., 45(2011), pp. 953-959

[16] Y. F. Ning, Y. P. Chen, S. Li, J. S. Guo, X. Gao, F. Fang , Y. Shen, K. Zhang, Development of an in situ dissolved oxygen measurement system and calculation of its effective diffusion coefficient in a biofilm, Anal. Methods, 4(2012), pp. 2242-2246

[17] R. S. Renslow, J. T. Babauta, P. D. Majors, H. Beyenal, Diffusion in biofilms respiring on electrodes, Energy Environ. Sci., 6(2013), pp. 595-607

[18] R. S. Renslow, J. T. Babauta, A. C. Dohnalkova, M. I. Boyanov, K. M. Kemner, P. D. Majors, J. K Fredrickson, H. Beyenal, Metabolic spatial variability in electrode-respiring Geobacter sulfurreducens biofilms, Energy Environ. Sci., 6(2013), pp. 1827-1836

[19] D. Sun, D. F. Call, P. D. Kiely, A. J. Wang, B. E. Logan, Biotechnol. Bioeng., Syntrophic interactions improve power production in formic acid fed MFCs operated with set anode potentials or fixed resistances, 109(2012), pp. 405–414

[20] K. P. Katuri, P. Kavanagh, S. Rengaraj, D. Leech, Geobacter sulfurreducens biofilms developed under different growth conditions on glassy carbon electrodes: insights using cyclic voltammetry, Chem. Commun., 46(2010), pp. 4758-4760

[21] J. Bard and L. R. Faulkner, 2010, Electrochemical Methods: Fundamentals and Applications, 2nd ed. Wiley, New York

[22] R. Renslow, J. Babautaa, A. Kupratb, J. Schenk, C. Ivorya, J. Fredricksond, H. Beyenal, Modeling biofilms with dual extracellular electron transfer mechanisms, Phys. Chem. Chem. Phys., 15(2013), pp. 19262-19283

[23] J. X. Hou, Z. L. Liu, ; P. Y. Zhang, A new method for fabrication of graphene/polyaniline nanocomplex modified microbial fuel cell anodes, J. Power Sources, 224(2013), pp. 139-144

[24] J. X. Hou, Z. L. Liu, S. Q. Yang, Y. Zhou, Three-dimensional macroporous anodes based on stainless steel fiber felt for high-performance microbial fuel cells. J. Power Sources, 258(2014), pp. 204-209

[25] Y. L. Ye, X. P. Zhu, B. E. Logan, Effect of buffer charge on performance of air-cathodes used in microbial fuel cells, Electrochimica Acta, 194, (2016), 441-447.

Figure Captions

Fig. 1 Growth of *Geobacter* biofilm under a constant applied potential (-0.1 V vs. Ag/AgCl). The red arrows indicate the various current densities for pH and CV measurements (they are1.07 A m^{-2}, 1.27 A m^{-2}, 2.58 A m^{-2}, 2.97 A m^{-2}, 4.46 A m^{-2}, 5.89 A m^{-2}, 7.93 A m^{-2}, 9.25 A m^{-2}, 9.83 A m^{-2}, 10.71 A m^{-2}, 10.23 A m^{-2} and 10.70 A m^{-2} for 45 h, 72 h, 116 h, 140 h, 205 h, 256 h, 285 h, 330h , 418 h, 440 h, 455 h and 482 h, respectively).

Fig. 2 Averaged pH distributions within *Geobacter* biofilm, the boundary layer and the bulk solution at current densities of 1.07 A m-2 and 1.27 A m^{-2} (a); 2.58 A m^{-2} and 2.97 A m^{-2} (b); 4.46 A m^{-2}, 5.89 A m^{-2} and 7.93 A m^{-2} (c); 9.25 A m^{-2} and 9.83 A m^{-2} (d); 10.71 A m^{-2}, 10.23 A m^{-2} and 10.70 A m^{-2} . And the error bars indicate the standard deviations. Fig. 2(f) is one of the profiles measured at 7.93A m^{-2} and its corresponding PC-depth profile above and within *Geobacter* biofilm.

Fig. 3 First derivative plots of the pH to the depth at 7.93 A m^{-2}, the inset figure presents the average curve and the error bars indicate the standard deviations. The calculated biofilm thickness is 275 μm (a); Thickness of *Geobacter* biofilm and its active part and inactive part at various current densities (b).

Fig. 4 pH variations near anode surface and in the bulk solution and as well as pH difference as a function of current density (a). Average pH variation curve within *Geobacter* biofilm and the corresponding proton concentration curve at various current densities, the inset displays the linear correlation between current densities and the average pH values (r^2 = 0.99) (b).

Fig. 5 First derivative plots (d*i*/d*V*) of CVs, the inset shows the midpoint potential variations as a function of the average pH levels within *Geobacter* biofilm.

Fig. 6 Effect of buffer concentration **(**25, 50, 75 and 100 mM**)** on pH distributions within *Geobacter* biofilm. And the error bars indicate the standard deviations.

Fig.1

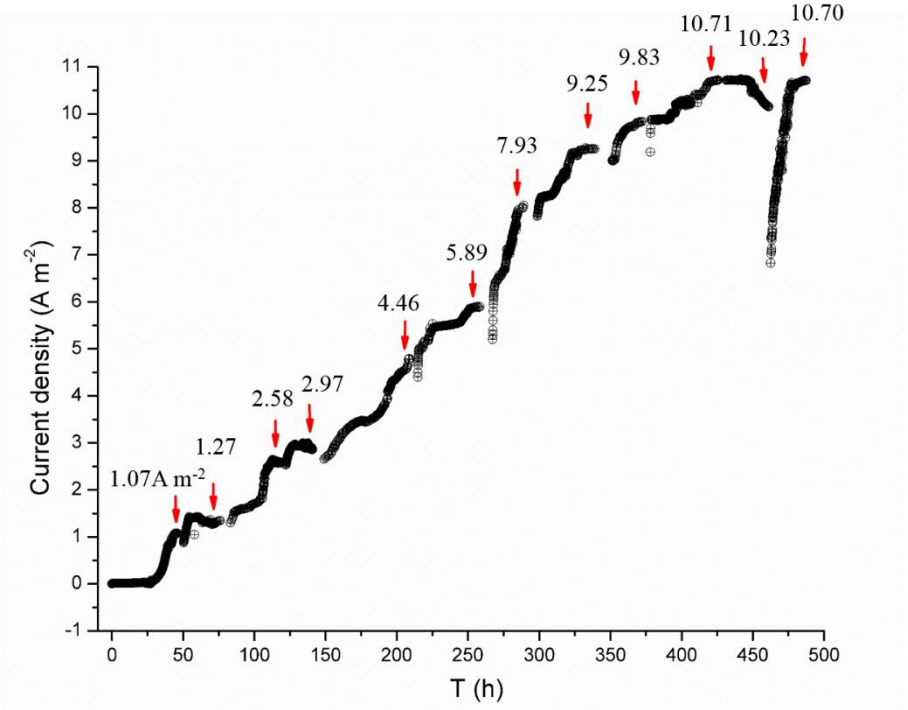

Fig. 2

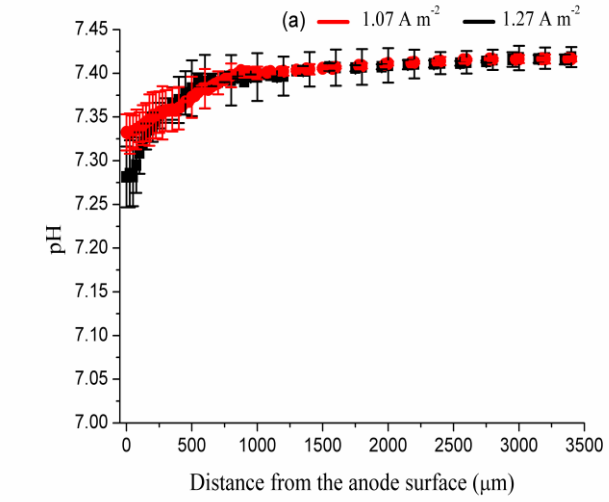

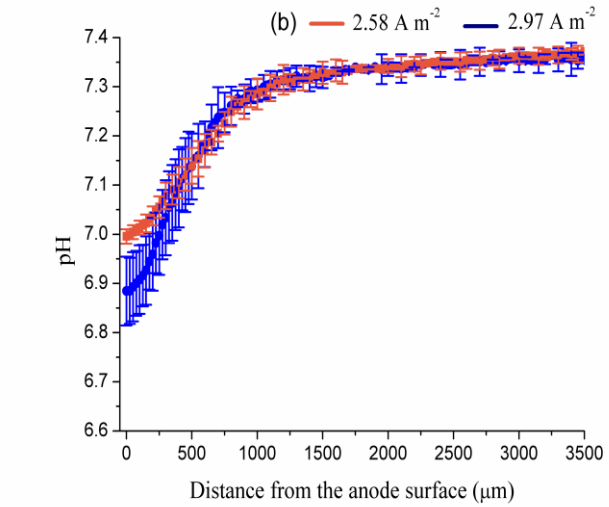

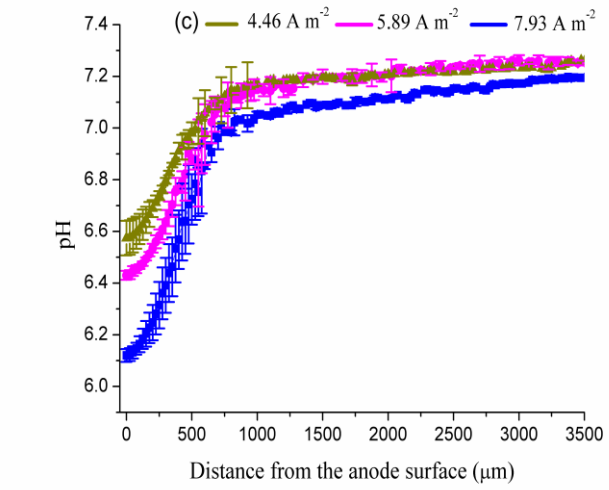

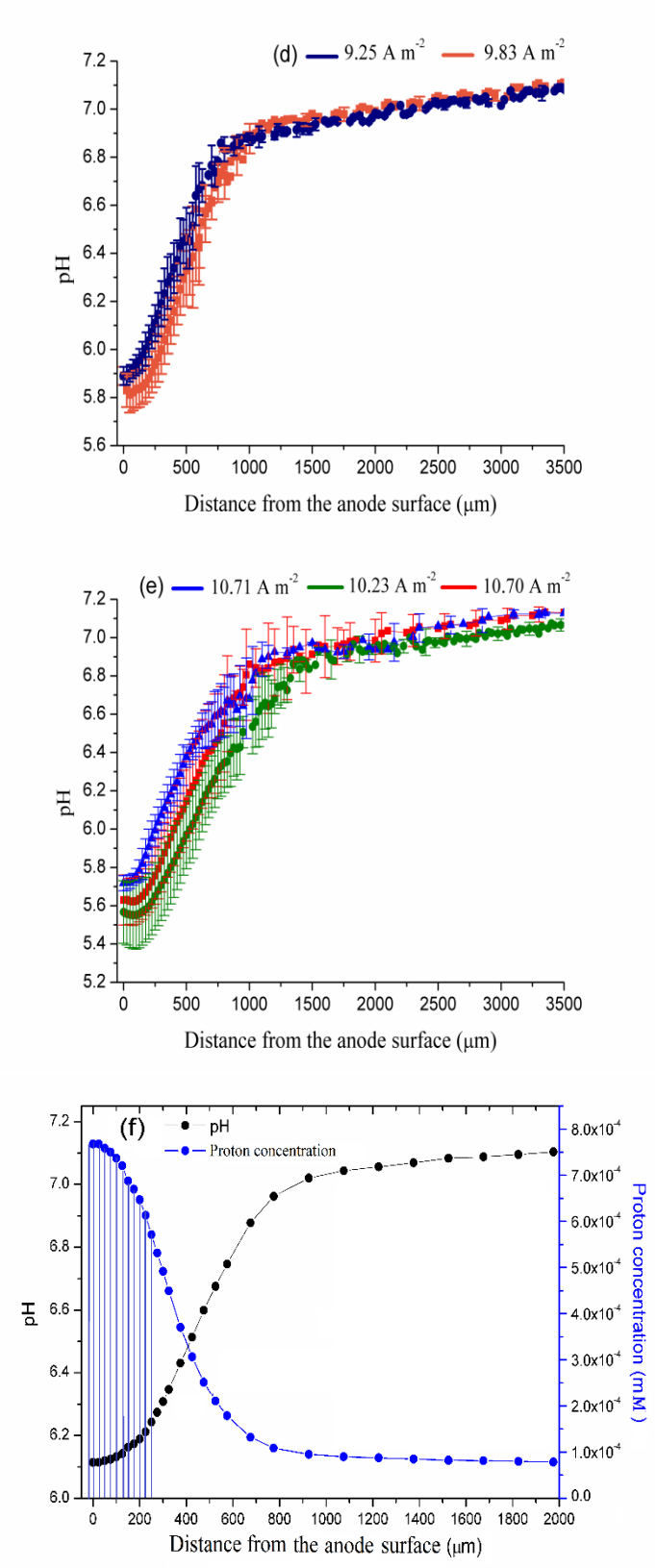

Fig.3

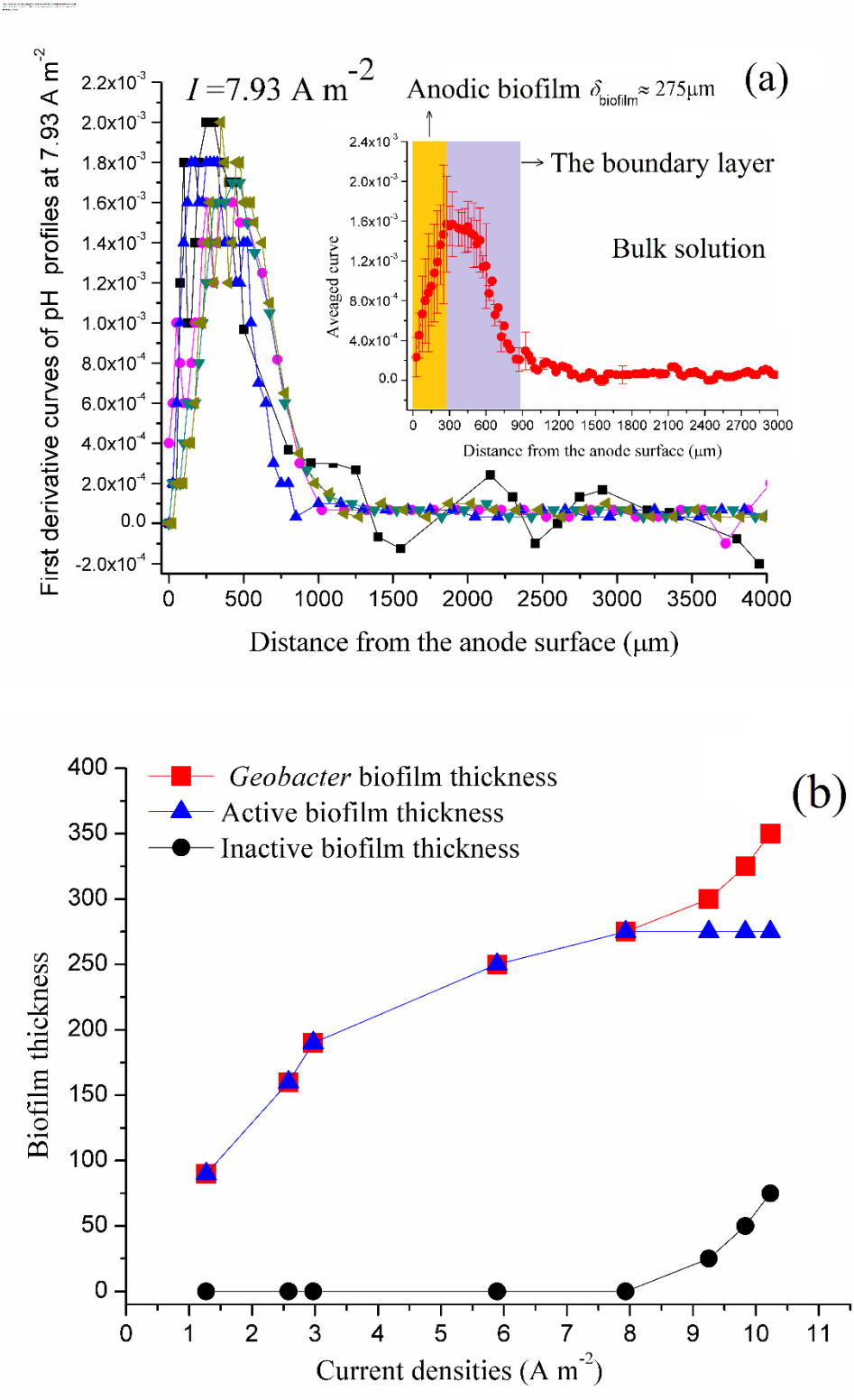

Fig. 4

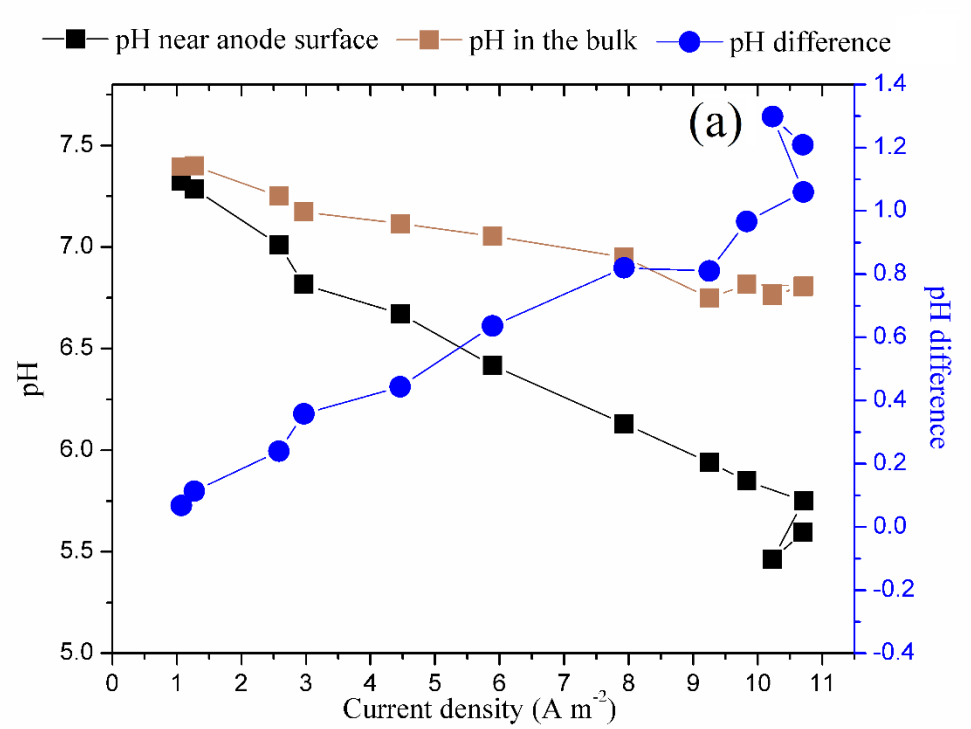

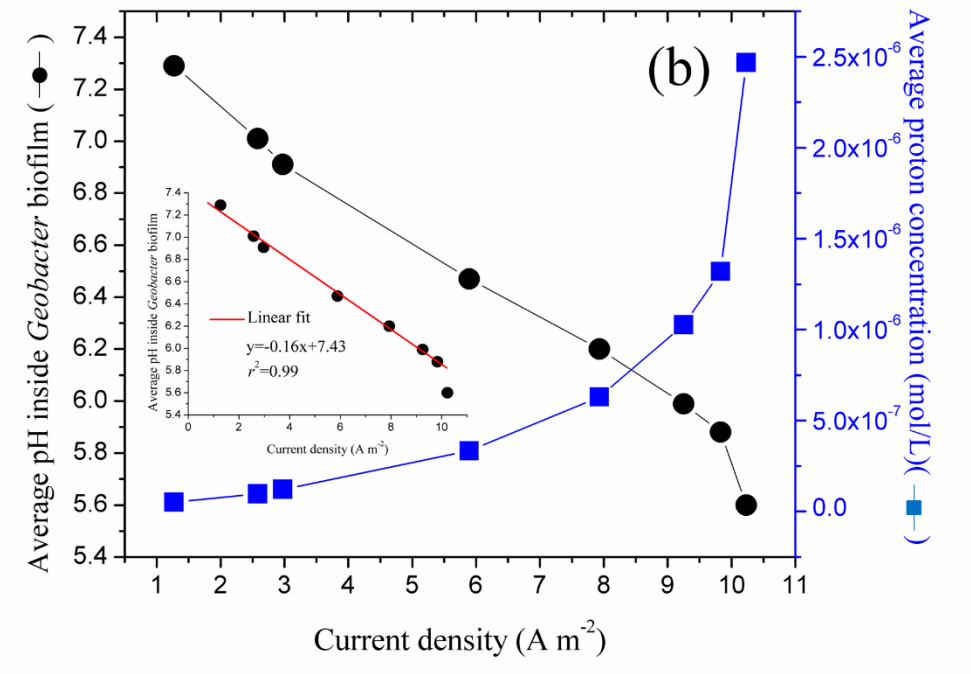

Fig. 5

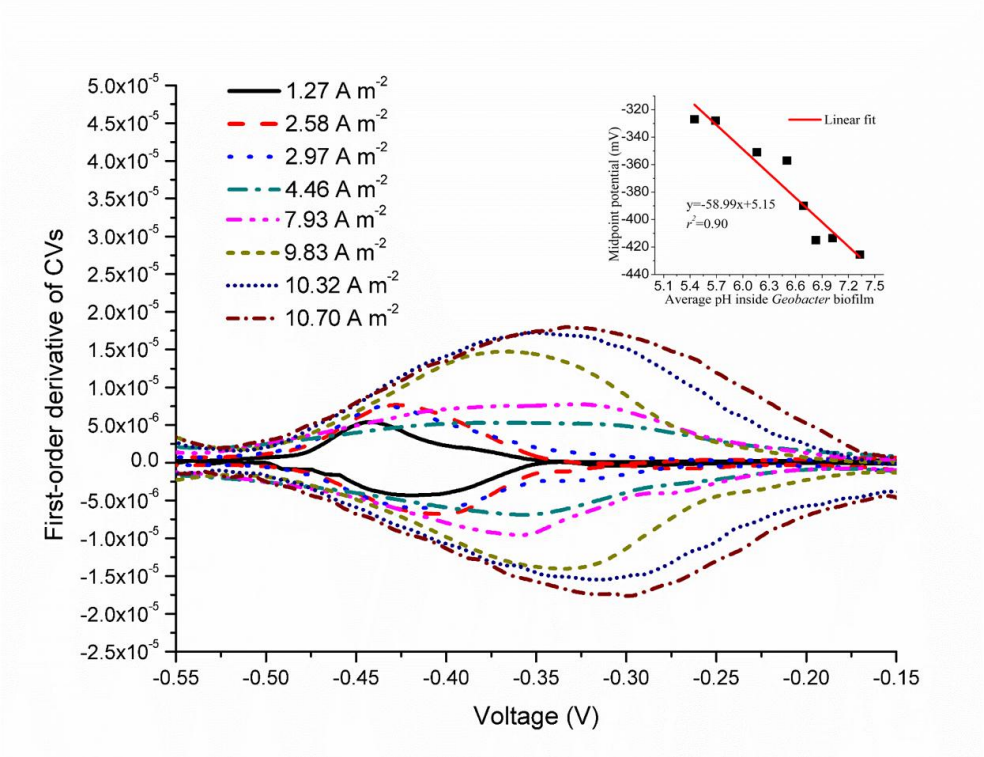

Fig 6